Inorganic Chemistry

Article

Structural Phase Transition of Gd$_3$RuO$_7$

Nobuo Ishizawa,* Kenji Tateishi, Saki Kondo, and Tsuyoshi Suwa

Ceramics Research Laboratory, Nagoya Institute of Technology, Tajimi, Gifu, Japan 507-0071

Structural phase transition of trigadorinium ruthenium heptaoxide, Gd$_3$RuO$_7$, has been investigated by in situ high-temperature single-crystal X-ray diffraction. A small shrinkage in *b*-length and an expansion in *c*-length were observed between 363 and 383 K with increasing temperature. No significant change occurred in *a*-length within experimental errors. The changes were essentially reversible against temperature. Structures of the high-temperature modification have been determined at 423, 773, and 1223 K assuming the orthorhombic *Cmcm* symmetry. The structure of the low-temperature modification has been determined at 293 K, assuming the orthorhombic *P2$_1$nb* symmetry with doubled unit cell along the *b*-axis of the high-temperature modification. The transition from high- to low-temperature modification can be structurally characterized by tilts about axes close to the *c*-axis of the unit cell occurring on half of the RuO$_6$ octahedra. These octahedral tilts couple with a reduction in coordination number of the Gd atom bridging the adjacent RuO$_6$ single chains along the *b*-axis. The present study also revealed the presence of structural disorder in the high-temperature *Cmcm* modification that had not been reported for the archetypal *Cmcm* structures of lanthanide ruthenates (Ln$_3$RuO$_7$) and osmates (Ln$_3$OsO$_7$) in the literature. The disorder includes a dynamical or static distribution of one-third of Gd atoms in the unit cell, which is presumably linked to the libration of the octahedral tilts about the axes close to *c*.

Introduction

The series of Ln$_3$MO$_7$ crystals composed of trivalent lanthanide (Ln) and pentavalent transition metal oxides is expected to possess quasi-one-dimensional electric conduction properties along the MO$_6$ octahedral single chains. Bontchev et al. grew single crystals of Gd$_3$RuO$_7$ by the flux method and suggested that the crystal has localized carriers in one-dimension with Mott variable range hopping along the octahedral single chains.[1] They also reported two phase transitions at 14.5 and 8 K relevant to the orderings of the Ru and Gd magnetic moments, respectively. Harada and Hinatsu found another transition at 382 K for Gd$_3$RuO$_7$ and reported, from the specific heat measurement, that the transition is of the first order.[2]

Crystals of the Ln$_3$MO$_7$ series have the defect-fluorite-type structure and show a polymorphism. The structure was first determined for La$_3$NbO$_7$ on the basis of the *Cmcm*

symmetry.[3] The phase transition between *P2$_1$nb* and *Cmcm* was first reported for Sm$_3$RuO$_7$ at 190 K and Eu$_3$RuO$_7$ at 280 K[4] and then for Sm$_3$OsO$_7$ at 235 K, Eu$_3$OsO$_7$ at 330 K, and Gd$_3$OsO$_7$ at 430 K.[5] The *Cmcm* structure is considered as archetypal, possessing the highest symmetry among the Ln$_3$RuO$_7$ polymorphs.[6] The room-temperature structure of Gd$_3$RuO$_7$ was first analyzed also assuming *Cmcm*,[1] which made it difficult to suppose the symmetry of the high-temperature modification of Gd$_3$RuO$_7$ above 382 K. Recently, the crystal structure of Gd$_3$RuO$_7$ at room temperature was reexamined and found to possess the *P2$_1$nb* symmetry.[7] The present study was thus undertaken to verify the phase transition of Gd$_3$RuO$_7$ by a precise single-crystal X-ray diffraction method. This paper also points out that the present *Cmcm* high-temperature structure of Gd$_3$RuO$_7$ has a

* To whom correspondence should be addressed. E-mail: ishizawa@nitech.ac.jp.

(1) Bontchev, R. P.; Jacobson, A. J.; Gospodinov, M. M.; Skumryev, V.; Popov, B.; Lorenz, V. N.; Meng, R. L.; Litvinchuk, A. P.; Iliev, M. N. *Phys. Rev. B* **2000**, *62*, 12235−12240.

(2) Harada, D.; Hinatsu, Y. *J. Solid State Chem.* **2002**, *164*, 163−168.

(3) Allpress, J. G.; Rossel, H. J. *J. Solid State Chem.* **1979**, *27*, 105−114.

(4) Gemmill, W. R.; Smith, M. D.; zur Loye, H-C. *Inorg. Chem.* **2004**, *43*, 4254−4261.

(5) Gemmill, W. R.; Smith, M. D.; Mozharivsky, Y. A.; Miller, G. J.; zur Loye, H-C. *Inorg. Chem.* **2005**, *44*, 7047−7055.

(6) Groen, W. A.; van Berkel, F. P. F.; IJdo, D. J. W. *Acta Crystallogr.* **1987**, *C43*, 2262−2264.

(7) Ishizawa, N.; Hiraga, K.; du Boulay, D.; Hibino, H.; Ida, T.; Oishi, S. *Acta Crystallogr. Sect. E* **2006**, *E62*, i13−i16.
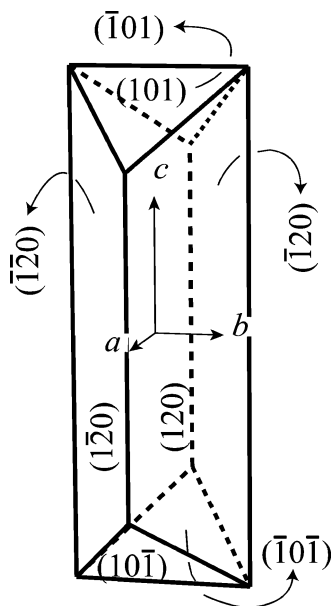
Figure 1. The face indices of typical as-grown crystal.

disordered nature and thus differs slightly from the archetypal *Cmcm* structures reported in the literature.

Experimental Section

Crystal Growth. Crystals were grown by cooling the $SrCl_2$–RuO_2–Gd_2O_3 solution at the rate of 5 K min^{-1} from 1373 K. The starting materials Gd_2O_3 (Japan Pure Chemical Co., 99.9%), RuO_2 (Japan Pure Chemical Co., 99.9%), and $SrCl_2$ (Japan Pure Chemical Co., 99%) were mixed together at the molar ratio 15:10:90 (total weight of approximately 5 g) and put into a 25 mL platinum crucible. The sample was heated in an electric furnace at 1373 K for 10 h in air atmosphere, cooled at the rate of 5 K h^{-1} to 973 K, and then cooled in the furnace to room temperature by turning off the power. The flux was washed away by distilled water. Metallic black crystals were found with average dimensions of 30 × 30 × 100 μm^3. Most of them had a prismatic shape surrounded by {120} side faces and capped by {101} as shown in Figure 1.

Single-Crystal X-ray Diffraction. Data were collected using a CCD single-crystal diffractometer (Smart Apex II, Bruker). A total reflection collimator was used to enhance the Mo Kα X-rays incident on the crystal.[8] A heating apparatus using hot nitrogen gas stream was attached to the diffractometer for experiments at high temperatures.[9] Three tiny crystals, I, II, and III, were used. Crystal I was mounted on a silica glass capillary with ceramic adhesive and used for data collection at relatively high temperatures of 773 and 1223 K. Crystal II was mounted on a soda glass capillary with epoxy resin for precise data collection at 293 and 423 K. Crystal III was mounted in a similar way as crystal I and used for measurements of cell dimensions and integrated intensities of reflections between 293 and 523 K at 20 K intervals upon heating and cooling. The precession images of various reciprocal lattice planes were reconstructed from the CCD frame data to examine the symmetry change of the crystal. The 0*kl* planes at 423 and 293 K are shown in Figure 2. The absorption correction was carried out by a numerical method taking the crystal shape into consideration. Data collection, extraction of observed structure factors, and
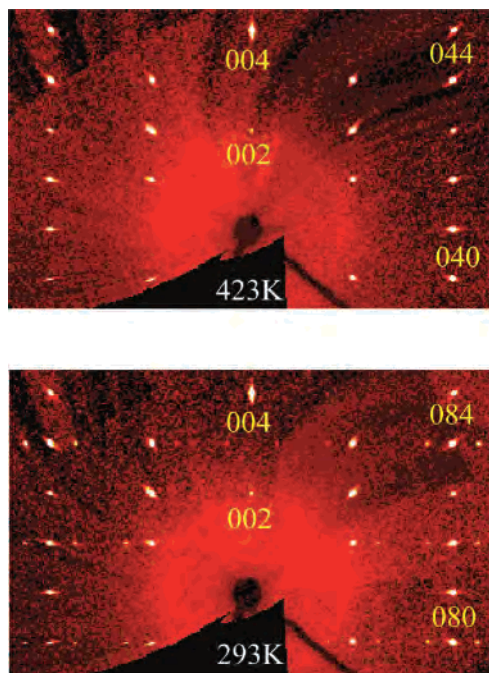

Figure 2. Precession images of the reciprocal 0*kl* plane at 423 K (*Cmcm*) and 293 K (*P2₁nb*) calculated from the three-dimensional CCD frame data.

absorption correction were carried out using the program package APEX2-W2K/NT.[10] Further calculations, including the least-squares refinements based on the structure factor (*F*), Fourier analysis, etc., were performed using the Xtal program package.[11] The extinction effect was corrected using the type I model proposed by Becker and Coppens.[12] ATOMS was used for drawing structures.[13]

Room-Temperature Structure. The structure at 293 K was determined using data collected up to 0.40 Å resolution level (2θ < 124°). The high-resolution analysis was essential to characterize the structural disorder of this type of compound, as pointed out for Tb_3RuO_7.[14] The unconstrained refinement of cell dimensions converged with interaxial angles of 90.000° ± 0.001° for 69 911 observed reflections. The agreement index of the symmetry equivalent reflections, R_{merge}, showed no significant improvement by reducing the Laue symmetry from *mmm* to lower ones. The crystal was thus assumed to have an orthorhombic symmetry. From the systematic absence of reflections, possible space groups were limited to $P2_1nb$ and *Pmnb*. The noncentrosymmetric $P2_1nb$ was adopted, because the mirror planes perpendicular to the *a*-axis in the centrosymmetric *Pmnb* do not allow octahedral tilts about the axes on the planes.

Since the origin of the unit cell can be taken at any point on the 2-fold screw axes of the space group $P2_1nb$, the *x* parameter of Ru1 is fixed at 0.0. The structure was essentially the same as that in the previous report.[7] However, as indicated by the Tb_3RuO_7 and Dy_3RuO_7 studies,[14,15] crystals of Gd_3RuO_7 were found to have a similar structural disorder regarding the positions of one-third of

(8) He, B. B.; Preckwinkel, U. *Adv. X-ray Anal.* **2002**, *45*, 332−337.
(9) Ishizawa, N.; Kondo, S.; Hibino, H.; Igarashi, S.; Nakamura, M.; Saho, R. *Annual Report of the Ceramics Research Laboratory 2006*, Nagoya Institute of Technology, 2007, *VI*, pp 12−18.
(10) *APEX−W2K/NT,* v1.0; Bruker Analytical X-ray Systems Inc.: Madison, WI, 2006.
(11) Hall, S. R.; du Boulay, D. J.; Olthof-Hazekamp, R., Eds. *The Xtal 3.7 System;* University of Western Australia: Perth, Australia, 2003.
(12) Becker, P. J.; Coppens, P. *Acta Crystallogr. Sect. A* **1974**, *A30*, 148−153.
(13) Dowty, E. *ATOMS for Windows,* V6.2; Shape Software, Kingsport, TN, 2005.
(14) Ishizawa, N.; Suwa, T.; Tateishi, K.; Hester, J. R. *Acta Crystallogr. Sect. C* **2007**, *C63*, i43−i46.
(15) Ishizawa, N.; Suwa, T.; Tateishi, K. *Acta Crystallogr. Sect. E* **2007**, *E63*, i163.

Table 1. Crystallographic Data and Structure Refinement for Gd₃RuO₇

formula	Gd$_3$RuO$_7$	Gd$_3$RuO$_7$	Gd$_3$RuO$_7$	Gd$_3$RuO$_7$
fw (g/mol)	684.82	684.82	684.82	684.82
temperature (K)	293	423	773	1223
wavelength (Å)	0.71073	0.71073	0.71073	0.71073
crystal system	orthorhombic	orthorhombic	orthorhombic	orthorhombic
space group	$P2_1nb$	$Cmcm$	$Cmcm$	$Cmcm$
unit cell dimensions				
a (Å)	10.6399(2)	10.6514(2)	10.6847(2)	10.7346(2)
b (Å)	14.6769(2)	7.3404(3)	7.3694(1)	7.4112(2)
c (Å)	7.3747(1)	7.3942(1)	7.4136(1)	7.4481(2)
volume (Å³)	1151.64(3)	578.12(3)	583.75(2)	592.54(3)
Z	8	4	4	4
density (Mg/m³)	7.899	7.868	7.792	7.676
abs coeff (mm⁻¹)	36.656	36.511	36.158	35.621
max sin θ/λ (Å⁻¹)	1.2422	1.2422	0.9945	0.9941
reflns collected	69911	96988	6299	6389
R_{merge}	0.053	0.060	0.028	0.030
absorption correction	numerical	numerical	numerical	numerical
indep reflns ($F > 3\sigma(F)$)	5547	1615	933	864
R based on F	0.035	0.028	0.028	0.032
wR based on F	0.029	0.019	0.029	0.025
weighting scheme	$1/\sigma^2(F)$	$1/\sigma^2(F)$	$1/\sigma^2(F)$	$1/\sigma^2(F)$
extinction coefficient	260(6)	137(8)	691(26)	750(23)
largest diff peak (e/Å³)	5.4 and −5.3	3.3 and −3.4	3.4 and −2.8	3.7 and −2.1

the Gd atoms. The split atom pair sites at A and B were assumed for both Gd1 and Gd2. The Gd atoms occupy either positions Gd1A or Gd1B with probabilities of approximately 92 and 8%, respectively. The distance between Gd1A and Gd1B is 0.36(2) Å. The Gd atoms also occupy either positions Gd2A or Gd2B with probabilities of approximately 93 and 7%, respectively. The distance between Gd2A and Gd2B is 0.46(1) Å. The high correlation between the probabilities 92−93% at the Gd1A and Gd2A sites may suggest a coexistence of major variants containing Gd atoms at the A sites and minor variants containing Gd atoms at the B sites in the crystals.

When no disorder was assumed for the Gd1 and Gd2 atoms, the refined positions of these atoms were very close to those of the Gd1A and Gd2A atom sites, respectively, with resultant residual peaks maximized 30 e/Å³ near the Gd1B and 19 e/Å³ near the Gd2B atom sites in the difference Fourier maps. The maximum residual peaks reduced to 5.4 e/Å³ in the final stage of refinement assuming the split-atom model. The Flack parameter was refined to 0.56(3) for the unmerged data set of the Friedel pairs.[16] The atom notations in this paper are different from our previous studies[7,14,15] and are reassigned in a way similar to the methods adopted by Gemmill et al.[4,5] published in this journal for comparison purpose. Details of the crystallographic data and structure refinements are given in Table 1. The atomic coordinates and the equivalent or isotropic atomic displacement parameters for the $P2_1nb$ modification at 293 K are given in Table 2.

High-Temperature Structure. The structure at 423 K was determined precisely using data up to the same resolution level of 0.40 Å as the 293 K data. From the extinction rules of reflections, possible space groups were limited to the centrosymmetric $Cmcm$ and noncentrosymmetric $C2cm$ and $Cmc2_1$ under the assumption of orthorhombic symmetry if the weak and diffuse intensities of $e0o$ reflections, where e and o stand for even and odd indices, respectively, were negligible, as detailed in a later section. After the least-squares procedure, the noncentrosymmetric $Cmc2_1$ structure model became almost identical to the centrosymmetric $Cmcm$ model. The $C2cm$ noncentrosymmetric model converged to a structure containing oddly shaped RuO₆ octahedra with some O atoms having unreasonably small atomic displacement parameters.

(16) Flack, H. D. *Acta Crystallogr. Sect. A* **1983**, *A39*, 876−881.

Table 2. Atomic Coordinates and Equivalent or Isotropic Atomic Displacement Parameters for the $P2_1nb$ Modification of Gd₃RuO₇ at 293 K

	x	y	z	population	$U_{eq}{}^a$ or U_{iso} (Å²)
Gd1A	0.0077(2)	0.13794(13)	0.50313(11)	0.918(8)	0.0065(1)*
Gd2B	0.0065(2)	0.11243(7)	0.00277(13)	0.082(8)	0.0069(1)*
Gd1B	0.0016(9)	0.1142(14)	0.4992(13)	0.925(6)	0.0065(1)*
Gd2B	0.0093(10)	0.1413(8)	−0.0067(12)	0.075(6)	0.0069(1)*
Gd3	0.2191(2)	0.47630(9)	0.76289(6)	1	0.0062(1)*
Gd4	0.2815(2)	0.22550(9)	0.74373(6)	1	0.0057(1)*
Gd5	0.2714(2)	0.52891(9)	0.25141(5)	1	0.0061(2)*
Gd6	0.2301(2)	0.27800(8)	0.24612(6)	1	0.0049(2)*
Ru1	0	0.37524(15)	0.4988(4)	1	0.0039(1)*
Ru2	−0.00160(7)	0.3295(6)	0.9983(4)	1	0.0039(1)*
O1	0.0025(8)	0.4145(6)	0.2503(6)	1	0.0063(11)
O2	−0.0121(8)	0.2832(5)	0.7490(6)	1	0.0048(11)
O3	0.1314(7)	0.2790(6)	0.5387(9)	1	0.0066(9)
O4	−0.1244(7)	0.4684(6)	0.5347(9)	1	0.0076(10)
O5	−0.1261(7)	0.4664(6)	0.4570(9)	1	0.0090(10)
O6	0.1286(7)	0.3049(5)	0.4642(9)	1	0.0074(10)
O7	0.1469(7)	0.4664(6)	−0.0494(10)	1	0.0134(11)
O8	−0.1069(6)	0.3049(5)	−0.0408(8)	1	0.0060(8)
O9	−0.1575(7)	0.4379(5)	0.0424(10)	1	0.0140(12)
O10	0.1034(8)	0.4828(6)	0.0407(10)	1	0.0128(13)
O11	0.3690(9)	0.3677(7)	0.7565(7)	1	0.0048(11)
O12	0.1307(11)	0.1180(8)	0.7641(10)	1	0.0091(15)
O13	0.1329(10)	0.1443(7)	0.2375(9)	1	0.0069(12)
O14	0.3648(10)	0.3941(7)	0.2349(9)	1	0.0075(12)

^{a} U_{eq} values are denoted with an asterisk.

Thus, the noncentrosymmetric models were discarded. The $Cmcm$ structure, however, is slightly different from those reported in the literature in that the Gd atom occupies one of the two crystallographically equivalent positions (8f in $Cmcm$) separated by 0.290-(1) Å with 50% probability. The nonsplit atom model in the literature, i.e., assuming the Gd1 atom is at the 4a position of $Cmcm$, converged to $R = 0.033$ with several problems: (a) the equivalent displacement parameter (U_{eq}) of Gd1 being 2.3 times larger than that of Gd2, (b) an extremely prolate ratio of 7.45 between the largest and smallest values along the principal axes of the displacement ellipsoid of Gd1 in comparison with 1.25 of Gd2, and (c) relatively large accumulation of residual electrons of 11 e/Å³ near Gd1 in the final difference Fourier map. All these features indicated that the nonsplit atom model was not acceptable. On the other hand, the split atom model used in the present study converged to $R = 0.028$, with U_{eq} of Gd1 being only 35% larger than Gd2, a

Table 3. Atomic Coordinates and Equivalent Atomic Displacement Parameters of the *Cmcm* Modification of Gd_3RuO_7 at 423, 773, and 1223 K[a]

	x	y	z	U_{eq} (Å²)
		423 K		
Gd1	0	0.01958(10)	−0.0020(2)	0.0115(2)
Gd2	0.22405(1)	0.30189(2)	0.25	0.00854(4)
Ru	0	0.5	0	0.00567(8)
O1	0.1265(2)	0.3139(3)	−0.0395(2)	0.0216(7)
O2	0.1328(2)	0.0259(3)	0.25	0.0109(7)
O3	0	0.4146(4)	0.25	0.0107(9)
		773 K		
Gd1	0	0.0204(3)	−0.0019(7)	0.0182(3)
Gd2	0.22442(3)	0.30159(4)	0.25	0.0140(1)
Ru	0	0.5	0	0.0089(1)
O1	0.1274(4)	0.3146(6)	−0.0390(5)	0.0314(11)
O2	0.1331(4)	0.0261(6)	0.25	0.0164(10)
O3	0	0.4140(9)	0.25	0.0170(14)
		1223 K		
Gd1	0	0.0226(2)	−0.0022(8)	0.0279(4)
Gd2	0.22501(3)	0.30100(4)	0.25	0.0233(1)
Ru	0	0.5	0	0.0150(1)
O1	0.1273(4)	0.3166(6)	−0.0392(5)	0.0471(13)
O2	0.1331(4)	0.0255(6)	0.25	0.0258(11)
O3	0	0.4145(10)	0.25	0.0287(18)

[a] The population of Gd1 is 0.5, whereas that of the others are 1.0.

mild prolate ratio of 3.08 for the Gd1 ellipsoid, and the residual electrons around Gd1 of less than 3.4 e/Å.³

The refinement of the structures at 773 and 1223 K was carried out in a similar way as that at 423 K. The split atom model for Gd1 was chosen for all the high-temperature data sets on the basis of the same reasons described above. Details of the crystallographic data and structure refinement are given in Table 1. The atomic coordinates and equivalent atomic displacement parameters for the *Cmcm* modification at 423, 773, and 1223 K are given in Table 3. Important geometry parameters of the low- and high-temperature modifications are summarized in Table 4. The volume, quadratic elongation, and angle variance[17] of the RuO_6 octahedra were calculated by PLATON.[18]

Scanning Electron Microscopy. Crystals were examined by the scanning electron microscope (JEOL JSM-7000F) with energy dispersive spectrometer (JEOL JED-2300). Gd, Ru, and O elements were detected. No impurities were found within the detection limit of the instrument.

Results and Discussion

Temperature dependences of cell dimensions in the range between 293 and 523 K are shown in Figure 3. A small shrinkage in *b*-length and an expansion in *c*-length were observed between the 363 and 383 K data points on heating and the reverse took place on cooling. Between these data points lies the phase transition temperature of 382 K reported from the specific heat measurement.[2] Thus, it was concluded that the observed anomalies of cell dimensions are associated with the structural phase transition of the compound at 382 K. The changes of cell dimensions suggest that the transition is reversible. The *a*-length changes monotonically, and no anomaly was observed within experimental errors.

Figure 4 shows the temperature dependence of the mean $|F_o|^2$ of eight reflection groups, *eoe*, *ooo*, *ooe*, *eoo*, 0*oo*, 0*oe*, *o*0*o*, and *e*0*o*, on the basis of the $P2_1nb$ lattice. The reflections in these groups can exist in $P2_1nb$ and should disappear in *Cmcm*. The data were collected on the crystal III on heating. The temperature dependence was essentially the same on cooling the specimen, suggesting again that the transition is reversible. The mean $|F_o|^2$ of the first seven groups, i.e., *eoe*, *ooo*, *ooe*, *eoo*, 0*oo*, 0*oe*, and *o*0*o*, decreased rapidly with increasing temperature and disappeared at data points above 382 K. The reflections of the group *e*0*o* were slightly stronger and more diffuse than those of the other seven groups above 382 K, although the $|F_o|^2$ value of the strongest reflection in the group *e*0*o* did not exceed 3 times its estimated standard uncertainty. They were thus neglected for the space group determination.

Some of the Ln_3MO_7 crystals, e.g., Ln_3MO_7 (M = Nb, Ta and Sb, Ln = Nd, Gd and Ho),[3] Y_3TaO_7,[19] and Dy_3ReO_7,[20] have been reported to crystallize in the space group $C222_1$. The space groups $C222_1$ and *Cmcm* can be distinguished from the *h*0*l* reflections, i.e., the reflection group *e*0*o* is allowed for $C222_1$ whereas not for *Cmcm*. The possibility of $C222_1$ was discarded for this crystal for the aforementioned reason.

The structure of the $P2_1nb$ modification at 293 K is illustrated in Figure 5. There are two crystallographically independent octahedra, $Ru1O_6$ and $Ru2O_6$. The two octahedra alternate along the *c*-axis by sharing the trans O atom, O_t, to form a zigzagging single chain of $[-Ru1O_5-Ru2O_5-]_\infty$. These single chains are embedded and separated from each other in a matrix consisting of Gd and O atoms. The $Ru1O_6$ octahedron has practically one tilt system about an axis parallel to the *a*-axis. On the other hand, the $Ru2O_6$ octahedron has a second tilt system about an axis close to the *c*-axis, in addition to the first tilt about the axis parallel to *a*. Hereafter, the first and second tilt systems are briefly noted as the tilt about *a* and the tilt about *c*, respectively.

The structure of the high-temperature *Cmcm* modification is illustrated in Figure 6. The two independent $Ru1O_6$ and $Ru2O_6$ octahedra in the $P2_1nb$ modification become crystallographically identical in *Cmcm*. The $Ru1O_6$ in the high-temperature form has a single tilt about *a*. The appearance and disappearance of the tilt about *c* for every other RuO_6 octahedron is a structural feature that characterizes the $P2_1nb-$*Cmcm* phase transition.

The RuO_6 octahedra are elongated along the chain in the high-temperature form as seen from the ratio of $\langle Ru-O_t \rangle_2/\langle Ru-O_c \rangle_4$ in Table 4, where O_c stands for the O atom in the cis position of octahedra with respect to O_t, and the angle brackets stand for taking an average over the number of bonds given as a subscript. The values of quadratic elongation and angle distortion in Table 4 suggest that the shape of oxygen octahedra in the high-temperature form resolves into more distorted $Ru1O_6$ and less distorted $Ru2O_6$ in the

(17) Robinson, K.; Gibbs, G. V.; Ribbe, P. H. *Science* **1971**, *172*, 567–570.
(18) Spek, A. L. *PLATON*; A Multipurpose Crystallographic Tool, Utrecht University, Utrecht, The Netherlands. 2007: *J. Appl. Crystallogr.* **2003**, *36*, 7–13.
(19) Rossell, H. J. *J. Solid State Chem.* **1979**, *27*, 115–122.
(20) Hinatsu, Y.; Wakeshima, M.; Kawabuchi, N.; Taira, N. *J. Alloys Compd.* **2004**, *374*, 79–83.

Table 4. Selected Interatomic Distances (Å) and Geometry Parameters[a]

	293 K		423 K	773 K	1223 K
$\langle Gd1A-O \rangle_7$ (Å)	2.420(9)	$\langle Gd1-O \rangle_8$ (Å)	2.513(2)	2.527(5)	2.537(5)
$\langle Gd1B-O \rangle_7$ (Å)	2.462(15)				
$\langle Gd2A-O \rangle_7$ (Å)	2.416(9)				
$\langle Gd2B-O \rangle_7$ (Å)	2.467(13)				
$\langle Gd3-O \rangle_7$ (Å)	2.391(9)	$\langle Gd2-O \rangle_7$ (Å)	2.363(2)	2.367(4)	2.372(4)
$\langle Gd4-O \rangle_7$ (Å)	2.366(9)				
$\langle Gd5-O \rangle_7$ (Å)	2.358(8)				
$\langle Gd6-O \rangle_7$ (Å)	2.364(8)				
$\langle Ru1-O \rangle_6$ (Å)	1.947(8)		1.945(2)	1.953(4)	1.948(4)
$\langle Ru1-O_t \rangle_2$ (Å)	1.945(8)		1.952(1)	1.959(2)	1.967(2)
$\langle Ru1-O_c \rangle_4$ (Å)	1.948(6)		1.941(2)	1.950(4)	1.949(4)
$\langle Ru1-O_t \rangle_2/\langle Ru1-O_c \rangle_4$	0.9985		1.0057	1.0046	1.0092
octahedral volume (Å^3)	9.744		9.738	9.857	9.897
quadratic elongation	1.006		1.005	1.005	1.005
angle variance	22.85		16.94	18.65	16.78
$\langle Ru2-O \rangle_6$ (Å)	1.949(7)				
$\langle Ru2-O_t \rangle_2$ (Å)	1.953(6)				
$\langle Ru2-O_c \rangle_4$ (Å)	1.947(8)				
$\langle Ru1-O_t \rangle_2/\langle Ru1-O_c \rangle_4$	1.0031				
octahedral volume (Å^3)	9.807				
quadratic elongation	1.004				
angle variance	14.63				
Ru1···Ru2 (Å)	3.683(4)	Ru1···Ru1 (Å)	3.6971(1)	3.7068(1)	3.7241(1)
	3.691(4)				
Ru1−O1−Ru2 (deg)	140.4(5)	Ru−O3−Ru (deg)	142.5(2)	142.2(4)	142.4(4)
Ru1−O2−Ru2 (deg)	144.1(5)				

[a] The interatomic distances (Å) in angle brackets are the average over the shortest n bonds with n given as a subscript. The O_t represents trans O atoms connecting the RuO_6 octahedra along the chain, and O_c represents the other cis O atoms of RuO_6 octahedra.
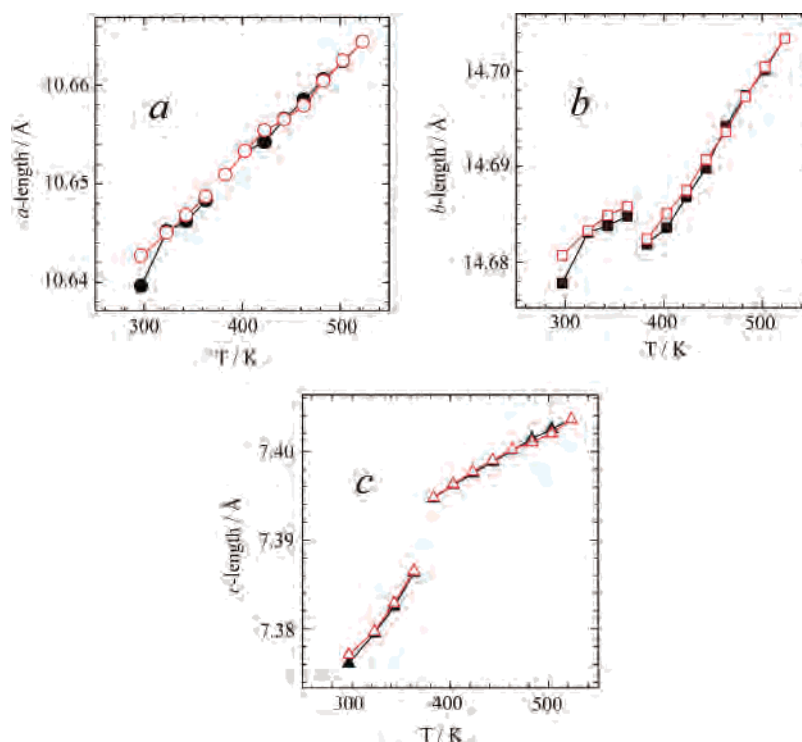

Figure 3. Temperature dependence of the a-, b-, and c-lengths of Gd_3RuO_7. Data points of filled black marks on heating and open red ones on cooling are connected by polylines for viewing purpose. The b-length of the *Cmcm* modification above 382 K is doubled in the figure for comparison with the low-temperature $P2_1nb$ modification. The estimated standard uncertainties of the cell lengths are less than the marker size.

low-temperature form. The Ru−O_t−Ru angle of 142.5° at 423 K is slightly more obtuse than the mean of the two Ru−O_t−Ru angles at 293 K in the low-temperature form, i.e., 140.4(5)° for Ru1−O1−Ru2 and 144.1(5)° for Ru1−O2−Ru2. This indicates that the octahedral single chain tends to unfold in the high-temperature form.

Along the chain, there is one kind of intermetallic Ru···Ru distance in the high-temperature form, corresponding to the half of the c length, whereas there are two kinds of Ru···Ru distances in the low-temperature form. The temperature dependence of the Ru···Ru distance is shown in Figure 7. The Ru···Ru distance in the high-temperature form is much
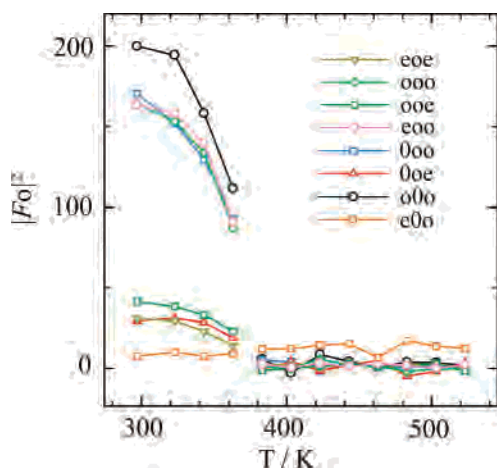
Figure 4. Temperature dependence of the mean $|F_o|^2$ of seven reflection groups, *eoe*, *ooo*, *ooe*, *eoo*, *0oo*, *0oe*, *o0o*, and *e0o*, where *o* and *e* stands for odd and even indices, respectively, on the basis of the $P2_1nb$ lattice. The data were collected on the crystal III on heating. The data points are connected by polylines in the high- and low-temperature forms for viewing purpose.
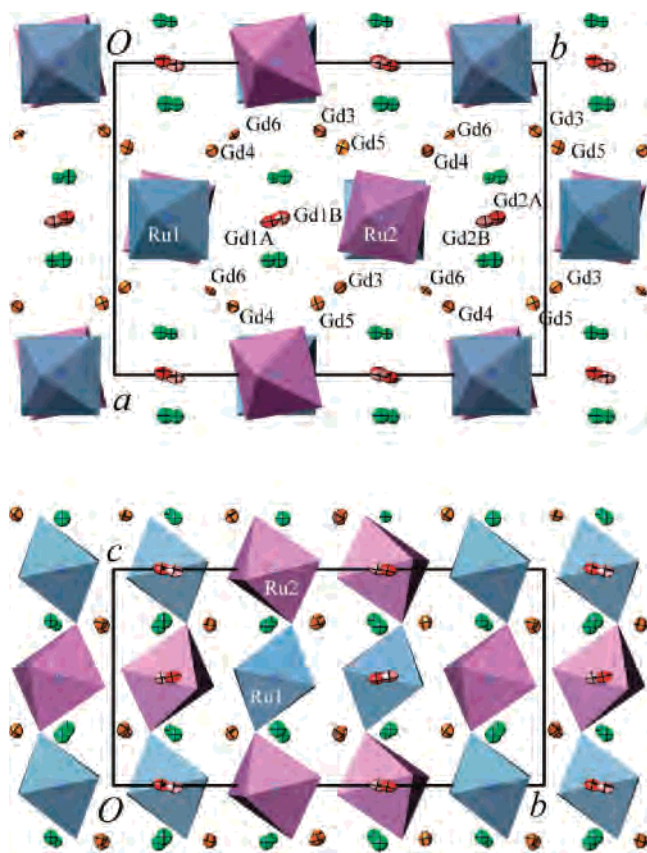

Figure 5. Structure of the $P2_1nb$ modification at 293 K viewed along *c* (upper) and *a* (lower) with atomic displacement parameter ellipsoids plotted at the 97% probability level.

Figure 6. Structure of the *Cmcm* modification at 423 K viewed along *c* (upper) and *a* (lower) with atomic displacement parameter ellipsoids plotted at the 97% probability level.

Figure 7. Changes of the intermetallic Ru···Ru distance along the RuO₆ chain with temperature. The estimated standard uncertainties are within the marker size. Two Ru···Ru distances in the $P2_1nb$ modification at 293 K lie below the dashed quadratic polynomial line connecting the values in the *Cmcm* modification at high temperatures.

larger than their mean in the low-temperature form. The elongation of octahedra, the unfolding tendency of the chain, and the increase of intermetallic Ru···Ru distance accord geometrically with each other. They also explain the shrinkage of the *b*-length and the expansion of the *c*-length (Figure 3) near the phase transition point on heating and vice versa on cooling. The inequality of Ru···Ru intermetallic distances along the chain in the low-temperature form, as shown in
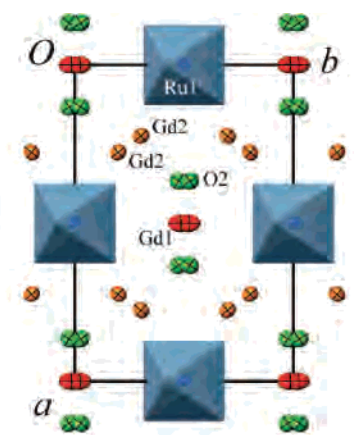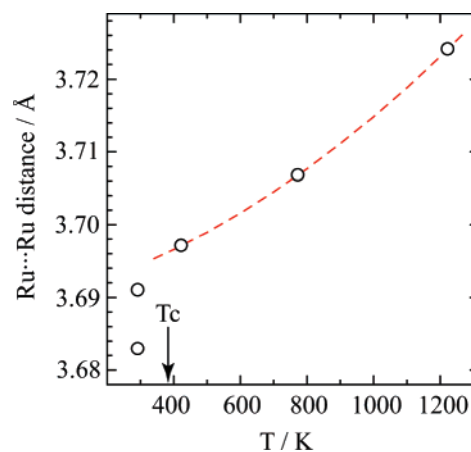
Figure 7, indicates that the dimerization of adjacent Ru atoms takes place in addition to the shortening of the Ru···Ru distances. This suggests a higher, and slightly different, electronic correlation between the Ru atoms along the chain in the low-temperature form compared with the high-temperature form. A detailed analysis of the band structure is necessary in order to understand the phase transition as well as the conduction properties.[1]
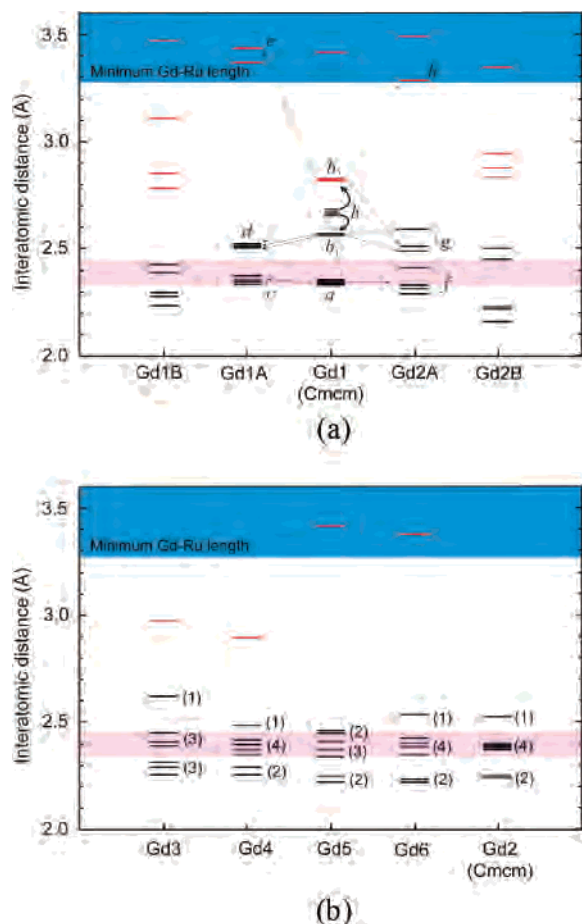
Figure 9. Geometrical relation between the RuO$_6$ octahedral tilts and reduction in coordination number of Gd atoms between the *Cmcm* (a) and *P*2$_1$*nb* (b) structures. The structural parameters at 423 and 293 K are used for drawing. The atomic displacement parameter ellipsoids are drawn at the 97% probability level.

also close to the pink band, whereas the bonds at b_2 could be eliminated from the coordination sphere of Gd atom. Thus, the coordination number of Gd1 can be considered as 6 or 6 + 2 instead of 8.

Below the phase transition temperature, the bonds at levels a and b_1 shift to level groups c and d for Gd1A and f and g for Gd2A. The two bonds at level b_2 split largely into d and e for Gd1A and g and h for Gd2A. The levels e and h lie in the blue area and are difficult to be considered as bonds. The coordination number of Gd1A and Gd2A thus becomes 7 in the low-temperature form, with the mean bond lengths lying in the pink band. The change in coordination number of Gd1 atom also characterizes the P2$_1$$nb$−$Cmcm$ transition in addition to the octahedral tilting about c.

The Gd1B and Gd2B atom sites have bonds with rather scattered distances, as shown in Figure 8a. They are surrounded by five O atoms at moderate levels colored in black and three O at distant levels in red. We will come to this topic later.

The atom sites of Gd3, Gd4, Gd5, and Gd6 in the low-temperature form become crystallographically equivalent Gd2 sites in the high-temperature form. The Gd atoms at the Gd2 site are surrounded by seven O atoms with the mean lying in the pink band, as seen in Figure 8b. The Gd3, Gd4, Gd5, and Gd6 atoms in the low-temperature form also have seven O atoms in the neighbor. The distances are scattered within a relatively wide region, whereas the means are still within the pink band. These Gd atoms do not seem to be involved strongly in the P2$_1$$nb$−$Cmcm$ phase transition.

The RuO$_6$ octahedral single chains are bridged with each other along the b-axis by the Gd1−O1 bonds, as shown in Figure 9. The bridging is symmetrical in the high-temperature form due to the presence of mirror planes perpendicular to the a-axis. The presence of mirrors prevents octahedral tilting about c. Below the transition temperature, Each Gd1 atom misses one bond to the RuO$_6$ octahedron enabling a tilt about c for every other RuO$_6$ octahedra. This is essentially the same as those reported for the P2$_1$$nb$−$Cmcm$ phase transitions in Sm$_3$RuO$_7$ and Eu$_3$RuO$_7$,[4] and Sm$_3$OsO$_7$, Eu$_3$OsO$_7$, and Gd$_3$-OsO$_7$.[5]

Figure 8. Distribution of interatomic distances of Gd1A−O, Gd1B−O, Gd2A−O, and Gd2B−O in the P2$_1$$nb$ modification at 293 K compared with Gd1−O in *Cmcm* at 423 K (a) and Gd3−O, Gd4−O, Gd5−O, and Gd6−O in the P2$_1$$nb$ modification compared with Gd2−O in *Cmcm* at 423 K (b). The bonds with the same distance are slightly shifted vertically for viewing purpose. The Gd⋯Ru intermetallic distances appear in the blue area above 3.28 Å. The upper and lower limits of the pink band indicate the distances calculated from the sum of Gd and O ionic radii in 6- and 8-fold coordinations, respectively. The interatomic Gd−O distances near the pink band are colored in black and the other long ones are in red. The number of bonds with similar distances is given in parenthesis in part b.

The coordination of O atoms around Gd is illustrated in Figure 8. The pink band in the figure is a measure of standard Gd−O bond distances, bounded by the values corresponding to the sum of ionic radii of O and Gd assuming eight and six coordinations, respectively.[21] The blue area is the region where Gd⋯Ru intermetallic distances appear. The A−B pairs of Gd1 and Gd2 atom sites in the low-temperature form become crystallographically equivalent Gd1 sites in the high-temperature form. The Gd1 atom in *Cmcm* has four short bonds with the same length (level a in Figure 8a) to O2. If the Gd1 atom is located at the nonsplit atom site (4a of *Cmcm*), the additional four long bonds to O1 would have the same length (level b). Since the Gd1 in *Cmcm* is actually located at the split atom site (8f of *Cmcm*), these archetype four long bonds at level b split into two pairs at b_1 and b_2. This suggests that the nonsplit Gd1 atom sites with the equivalent four distant O2 atoms at level b are unstable. The level a lies at the bottom of the pink band. The level b_1 is
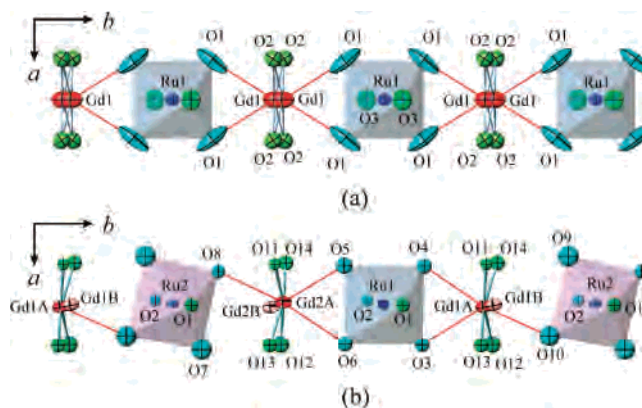
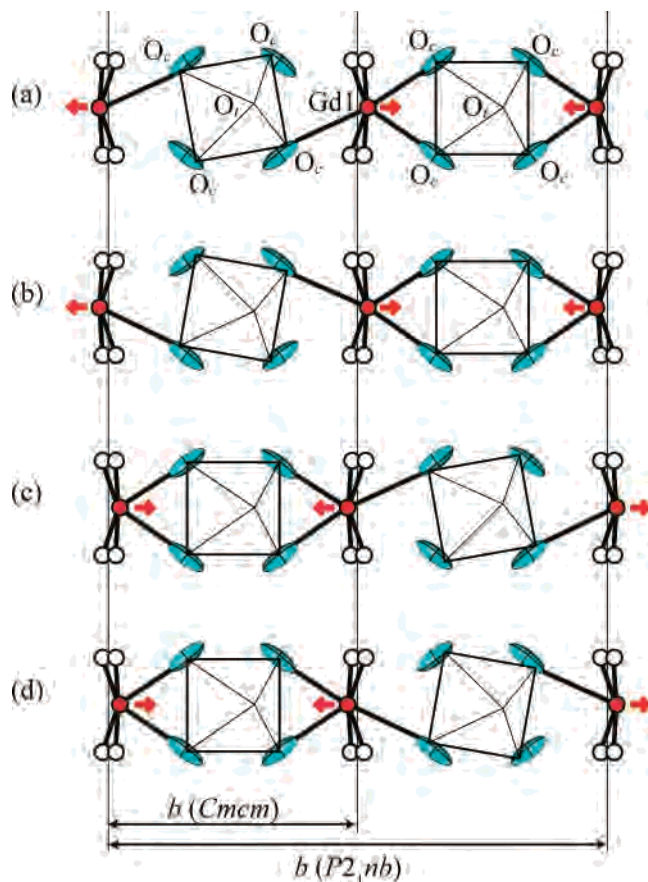(21) Shannon, R. D. *Acta Crystallogr. Sect. A* **1976**, *A32*, 751−767.

Figure 10. Four alternative hypothetical structures connecting Gd atoms and Ru(O$_c$)$_4$(O$_t$)$_2$ octahedra along the *b*-axis in the high-temperature form. The Gd1 atom is shown by a circle filled in red with an arrow indicating the direction of its displacement vector from the center of the split pair. The Gd1−O bonds are drawn by thick solid lines. The original prolate atomic displacement parameter ellipsoids of O1 atoms of the *Cmcm* modification are superimposed near O$_c$.

In the high-temperature *Cmcm* structures at 423, 773, and 1223 K, the distance of the Gd atom split pair is approximately 0.3 Å and does not show any significant temperature dependence. The atomic displacement parameters increase almost linearly as a function of temperature. It is notable that only the O1 atom has an extremely prolate atomic displacement parameter ellipsoid, as the overlapped Gd1 split pair looks like in Figure 9a.

The coordination geometry around Gd1 can vary depending on the actual Gd1 atom location in the spilt pair. Figure 10 illustrates four possible geometries in the high-temperature form. The directions of Gd1 atom shifts are the same in parts a and b and are reversed in parts c and d. The Gd1 atom is coordinated by two O$_c$ atoms of an octahedron by occupying a closer position to the octahedron. On the other hand, the shift provides to the other adjacent octahedron one of the two possible tilts (clockwise or counterclockwise) about the axes close to *c*, by releasing one Gd1−O$_c$ bond. Depending on the directions of Gd1 atom shifts, half of the octahedra tilt, whereas the remaining half remain untilted. The geometries of parts c and d have the antiphase relation against parts a and b along the *b*-axis, respectively.

The high-temperature *Cmcm* structure can be considered as a superposition of these four geometries. Although each

geometry has a doubled periodicity of the *Cmcm* structure along the *b*-axis, the superposition makes it halved. The O$_c$ atoms are located at the corners of clockwise-tilted, counterclockwise-tilted, and untilted octahedra. Superposing all the possible geometries would then make the probability density distribution of O$_c$ rather complicatedly elongated along the line connecting the octahedral corners. Such distribution is difficult to analyze on the basis of a simple split atom model for O$_c$. It is also suggested that these four geometries exist in the high-temperature form not statically but dynamically, because the phase transition at 482 K prescribes these geometries to get ordered in the low-temperature form. In this sense, the $P2_1nb$−*Cmcm* phase transition could be regarded as an order−disorder transition of the librating [−Gd−RuO$_6$−Gd−RuO$_6$−Gd−] linkage. This is consistent with the study of the specific heat measurement.[2] The present time-averaged X-ray analysis assumes simple harmonic vibrations for constituent atoms. The prolate feature of O1 ellipsoids thus obtained in the high-temperature form, however, may flag the presence of such a complicated dynamical distribution of O1 atoms. The vibrational mode analysis would be a future subject for better understanding of the disorder in the high-temperature form and the phase transition.

The low-temperature modification is noncentrosymmetric and has a primitive cell with doubled volume compared with the *C*-base centered centrosymmetric high-temperature modification. This means that eight possible variants can be generated in the low-temperature form, four of which are the antiphase variants of the remainder. Since the high-temperature form can be considered as a sort of dynamical mixture of four geometries, as shown in Figure 10, inclusion of various variants in the low-temperature form may be unavoidable. As already mentioned, a small fraction of Gd atoms was observed to exist statistically at the Gd1B and Gd2B sites. If there is no disorder about O atoms, Gd1B and Gd2B are surrounded by five O atoms with relatively short distances, as depicted in Figure 8a. The fraction of Gd atoms at Gd1B and Gd2B is 2.6% of the total Gd atoms in the unit cell. The fraction of neighboring O atoms around Gd1B and Gd2B are estimated to be 5.6% of the total O atoms in the unit cell. Taking into consideration the light-scattering power of the O atom and the complexity of the low-temperature form structure, it seems difficult to detect experimentally the positional disorder of such O atoms. The disorder at Gd1B and Gd2B could be rather ascribed to the trace presence of antiphase variants frozen into the low-temperature form crystal.

Gemmill et al.[4] mentioned that the refinement of the *Cmcm* modifications of Eu₃RuO₇ turned out a poorer fitting than that of Sm₃RuO₇. The anisotropic atomic displacement parameters of Sm1 and Eu1 atoms in these compounds are approximately 4-times prolate along *b*, and the values for Eu1 are approximately 50% larger than those for Sm1. This may indicate that the harmonic approximation of a nonsplit Ln1 atom model becomes less appropriate for describing the *Cmcm* structure with decreasing ionic radii in the sequence of Ln = Sm^{3+} (4f^5), Eu^{3+} (4f^6), and Gd^{3+} (4f^7).

The $P2_1nb$ modifications have been found recently for Ln_3-RuO_7 [Ln = Tb^{3+} ($4f^8$), Dy^{3+} ($4f^9$)] at room temperature.[14,15] They are also expected to undergo the $P2_1nb-Cmcm$ phase transition at high temperatures. If the known phase transition temperatures are plotted against ionic radii of Ln atoms, similar transitions are expected to occur at roughly estimated temperatures of 440 K for Tb_3RuO_7 and 510 K for Dy_3RuO_7. The disorder in the high-temperature form is also expected for the Tb and Dy compounds.

Summary

Crystals of Gd_3RuO_7 undergo a structural phase transition between the $P2_1nb$ and $Cmcm$ modifications at around 382 K. The transition is reversible and structurally characterized by an additional tilt about c that occurs in the low-temperature form for half of the RuO_6 octahedra in association with a reduction of coordination number from $6 + 2$ or 8 to 7 for one-third of the Gd atoms. The elongation of octahedra, the unfolding tendency of the $[-RuO_5-]_\infty$ zigzagging chain along c, and the resultant increase of the intermetallic Ru$\cdots$Ru distance explain a shrinkage of the b-length and an expansion of the c-length near the phase transition point on heating and vice versa on cooling. The transition is similar to those given in the literature for Sm_3RuO_7, Eu_3RuO_7, Sm_3OsO_7, Eu_3OsO_7, and Gd_3OsO_7, except that one of the crystallographically independent Gd atoms in the high-temperature $Cmcm$ modification is statically or dynamically distributed between two positions located very close with each other. The disordered distribution of the Gd atom in the high-temperature form is presumably correlated with the octahedral tilts about c, resulting in the experimental observation of an extremely prolate atomic displacement ellipsoid for the O1 atom in the cis position along the chain. The $P2_1nb-Cmcm$ phase transition can be considered as an order$-$disorder transition of the librating $[-Gd-RuO_6-Gd-RuO_6-Gd-]$ linkage. Similar phase transitions are expected to occur in Ln_3RuO_7 (Ln = Tb, Dy) with smaller Ln cation sizes at higher temperatures than Gd_3RuO_7.

Supporting Information Available: Additional structural and crystallographic data. The material is available free of charge via the Internet at http://pubs.acs.org.

IC701732D